

Toward Unified Control of a Powered Prosthetic Leg: A Simulation Study

David Quintero, *Student Member, IEEE*, Anne E. Martin, and Robert D. Gregg, *Senior Member, IEEE*

Abstract—This brief presents a novel control strategy for a powered knee-ankle prosthesis that unifies the entire gait cycle, eliminating the need to switch between controllers during different periods of gait. A reduced-order Discrete Fourier Transformation (DFT) is used to define virtual constraints that continuously parameterize periodic joint patterns as functions of a mechanical phasing variable. In order to leverage the provable stability properties of Hybrid Zero Dynamics (HZD), hybrid-invariant Bézier polynomials are converted into unified DFT virtual constraints for various walking speeds. Simulations of an amputee biped model show that the unified prosthesis controller approximates the behavior of the original HZD design under ideal scenarios and has advantages over the HZD design when hybrid invariance is violated by mismatches with the human controller. Two implementations of the unified virtual constraints, a feedback linearizing controller and a more practical joint impedance controller, produce similar results in simulation.

I. INTRODUCTION

To improve amputee gait, powered prosthetic legs are in development [1]–[3]. Several control methods have been proposed for these devices, but almost all of them divide the gait cycle into multiple, sequential periods with different controllers [4]. In the most common approach, a finite state machine switches between joint impedance controllers based on the period of gait [2]–[9]. Multiple ambulation modes can be handled by a combination of finite state machines with task-specific impedance controllers [10]. This approach requires substantial tuning of control parameters and switching rules for each period and task, potentially taking several hours to configure a powered knee-ankle prosthesis for a single amputee patient [11]. When perturbed, this control approach could switch to the wrong state and use the wrong controller, which may increase an amputee’s risk of falling.

These different periods of gait could potentially be unified by virtual kinematic constraints that are enforced using a torque control scheme [12]–[19]. Virtual constraints typically define desired joint trajectories as polynomial functions of a mechanical phasing variable. A phase variable is a kinematic quantity corresponding to an unactuated degree of freedom

that evolves monotonically during steady walking, thus representing the progression through the gait cycle. This phase-based control method was originally developed to control underactuated bipedal robots, such as MABEL [13], ERNIE [14], and ATRIAS [15]. If the biped is pushed forward (or backward), the phase variable increases (or decreases), which in turn speeds up (or slows down) the step. The controller is therefore able to automatically react to disturbances, which increases the robustness of the gait. This would be advantageous for a prosthesis controller by allowing the prosthesis to react to disturbances in a predictable manner that may resemble the response of a human leg [20], [21].

Virtual constraints for biped robots are currently defined in a piecewise manner, separated by stance-to-swing transitions. These transitions are typically modeled as discontinuous impact events when designing the piecewise virtual constraints. The method of Hybrid Zero Dynamics (HZD) encodes joint trajectories into polynomial functions that are invariant to these impact events (i.e., *hybrid invariant*), allowing a restriction of the hybrid dynamical system to the lower-dimensional HZD manifold for stability analysis [12]. This partial unification of the gait cycle and its provable stability properties have motivated recent work in virtual constraint control of powered prosthetic legs [22]–[24], which similarly define separate controllers for the stance and swing periods.

In contrast, humans move in a smooth, continuous manner over a periodic gait cycle. This smooth periodicity is lost across the discrete transitions of a finite state machine, even one that separates only stance and swing. To enable better control of powered prostheses, we propose a new class of virtual constraints that continuously parameterize periodic joint patterns based on the Discrete Fourier Transformation (DFT) [25]. These virtual constraints are defined from reduced-order frequency representations of the desired joint trajectories. Piecewise HZD polynomials for the knee and ankle are converted into unified DFT functions to leverage the provable stability properties of HZD while respecting the continuous, periodic nature of human walking. The DFT virtual constraints unify prosthetic control within the gait cycle and across gait cycles by repeating periodically over the phase variable.

Previous attempts at unified control of powered prosthetic and orthotic devices have used data-driven joint patterns and/or a single actuator. The powered prosthetic ankle in [1] tracks able-bodied human data as a function of a tibia-based phase angle throughout the gait cycle. Our approach differs by defining a torque control law to enforce HZD-inspired virtual constraints, which are easily generated for multiple joints and tasks with provable stability properties [12], [23], [24]. The

D. Quintero and R.D. Gregg are with the Departments of Bioengineering and Mechanical Engineering, University of Texas at Dallas, Richardson, TX 75080. A.E. Martin is with the Department of Mechanical and Nuclear Engineering, Pennsylvania State University, State College, PA 16801. dxq130330@utdallas.edu, rgregg@ieee.org

This work was supported by the National Institute of Child Health & Human Development of the NIH under Award Number DP2HD080349. The content is solely the responsibility of the authors and does not necessarily represent the official views of the NIH. R. D. Gregg holds a Career Award at the Scientific Interface from the Burroughs Wellcome Fund.

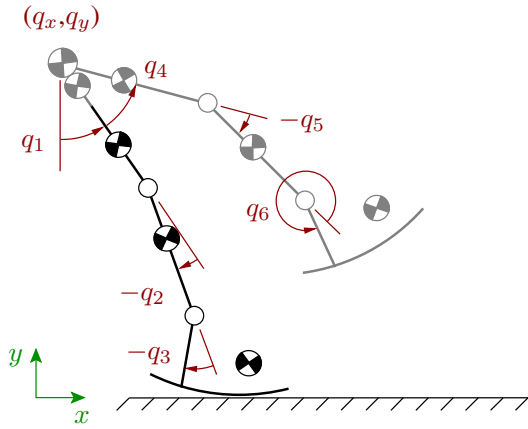


Fig. 1. Schematic of the unilateral, transfemoral amputee model (reproduced from [23], [24]). The prosthesis is shown in black and the human is shown in gray. The generalized coordinates used in the model are indicated with q terms. Angle q_1 is unactuated and angles q_{2-6} have ideal actuators.

hip exoskeleton in [26] uses a phase variable to determine when to inject or dissipate energy in the gait cycle, which may not be sufficient to replicate joint kinematics in a prosthesis application. In contrast, virtual constraints produce the desired kinematics in the absence of biological limb motion.

This brief presents the design and simulation of a unified prosthesis controller that continuously parameterizes periodic knee and ankle patterns across gait cycles. We begin with definitions of the amputee biped model and torque control methods for virtual constraints in Section II. After formulating unified virtual constraints by DFT in Section III, we describe the conversion of piecewise HZD designs into the unified framework. The simulations of Section IV demonstrate the ability of the unified controller to generate walking gaits that closely match the reference HZD gaits at various design speeds. The benefits of the unified design become clear when hybrid invariance of the piecewise HZD design is violated due to a mismatch with the human controller, specifically in the design speed. These results extend the preliminary work in [27] in three ways: comparing the robustness of piecewise HZD and unified DFT methods to mismatches with the human controller, demonstrating orbital stability of the unified gaits using the method of Poincaré, and demonstrating feasibility with a model-independent impedance controller. We summarize these contributions and future work in Section V.

II. MODELING AND CONTROL METHODS

This section reviews the methods used to model and control an amputee biped. After describing the hybrid dynamics of the biped model, we introduce the concept of virtual constraints with two torque control methods for enforcing them. These methods will later serve as the basis for the design and simulation of unified virtual constraints for a prosthetic leg.

A. Model

In this brief we consider the case of a unilateral, transfemoral amputee walking with a powered knee-ankle prosthesis. The planar biped model (Fig. 1) consists of seven

leg segments plus a point mass at the hip to represent the upper body as in [23], [24]. The thigh and shank segments are modeled using rigid links with mass and inertia. Model parameters are based on [28] with a leg length of 0.91 m and total mass of 68.5 kg. The full model is divided into a prosthesis subsystem consisting of the prosthetic thigh, shank, and foot, and a human subsystem consisting of the contralateral thigh, shank, and foot, the residual thigh on the amputated side, and the point mass at the hip. It is assumed that the prosthetic thigh and residual human thigh are rigidly attached, so the interaction forces between them are equal and opposite. Rather than model all of the contact phases and degrees of freedom of the foot, the function of the foot and ankle is modeled continuously using a circular foot [29], [30] plus an ankle joint to capture the stance ankle's positive work [28]. This foot model assumes rolling point contact, about which there is zero moment, so the ground reaction forces only contain tangential and normal components. Moreover, because the foot rolls without slip, the absolute angle q_1 is unactuated.

To describe the position and velocity of the biped, each subsystem has its own set of generalized coordinates. The configuration of each subsystem is described by the unactuated angle q_1 , the Cartesian coordinates (q_x, q_y) of the hip, and the relative angles of the actuated joints. The actuated joint angles for the entire biped are q_2 to q_6 . Thus, the generalized coordinates are $q_P = [q_1, q_2, q_3, q_x, q_y]^T$ for the prosthesis and $q_H = [q_1, q_4, q_5, q_6, q_x, q_y]^T$ for the human. Moreover, ideal actuators produce joint torques $u_P = [u_2, u_3]^T$ for the prosthesis and $u_H = [u_4, u_5, u_6]^T$ for the human.

For simulation, a stride starts just after the transition from contralateral stance to prosthesis stance and proceeds through the prosthesis stance period, an impact event, the contralateral stance period, and a second impact. The two stance periods can be modeled with continuous, second-order differential equations, and the two impact periods can be modeled using an algebraic mapping that relates the state of the biped at the instant before impact to the state of the biped after impact.

The equations of motion during the single-support period for each subsystem can be written as [23], [24]

$$M_i \ddot{q}_i + C_i \dot{q}_i + N_i - E_i^T G_i = B_i u_i + J_i^T F, \quad (1)$$

where subscript i indicates the subsystem (P for the prosthesis and H for the human), q_i are the subsystem coordinates, M_i is the inertia matrix, C_i is the matrix containing the centripetal and Coriolis terms, N_i contains the gravity terms, E_i is a contact constraint matrix, G_i is the two-dimensional vector of the ground reaction forces, B_i relates the input torques to the generalized coordinates, J_i is the Jacobian matrix relating the socket interaction forces to the generalized coordinates, and F is the three-dimensional vector of interaction forces.

Solving for \ddot{q}_i from the equations of motion (Eq. 1) gives

$$\ddot{q}_i = M_i^{-1} (-C_i \dot{q}_i - N_i) + M_i^{-1} B_i u_i + M_i^{-1} J_i^T F + M_i^{-1} E_i^T G_i. \quad (2)$$

Eq. 2 can also be written as a first-order state-space realization of the nonlinear system:

$$\dot{x}_i = f_i(x_i) + g_i(x_i) u_i + p_i(x_i) F + r_i(x_i) G_i, \quad (3)$$

where

$$\begin{aligned} x_i &= \begin{bmatrix} q_i \\ \dot{q}_i \end{bmatrix}, & f_i(x_i) &= \begin{bmatrix} \dot{q}_i \\ -M_i^{-1}(C_i\dot{q}_i + N_i) \end{bmatrix}, \\ g_i(x_i) &= \begin{bmatrix} 0 \\ M_i^{-1}B_i \end{bmatrix}, & p_i(x_i) &= \begin{bmatrix} 0 \\ M_i^{-1}J_i^T \end{bmatrix}, \\ r_i(x_i) &= \begin{bmatrix} 0 \\ M_i^{-1}E_i^T \end{bmatrix}. \end{aligned}$$

The generalized coordinates x_i are the states for the first-order nonlinear system (Eq. 3) with $f_i(x_i)$, $g_i(x_i)$, $p_i(x_i)$ and $r_i(x_i)$ as the vector field functions defining the full dynamic system.

The impacts can be modeled using equations of the form

$$q_i^+ = q_i^-, \quad \dot{q}_i^+ = A_i\dot{q}_i^- + \Lambda_i\mathcal{F}, \quad (4)$$

where \mathcal{F} is the socket interaction impulse that depends on the pre-impact state of both subsystems, and A_i and Λ_i are known matrices [23]. The superscripts ‘-’ and ‘+’ refers to the instants before and after impact, respectively.

B. Virtual Constraint Control

Virtual constraints encode the desired motions of actuated variables in output functions to be zeroed through control [12]:

$$y_{ij} = h_{ij}(q_i) = H_{0i}q_i - h_{ij}^d(\theta_i(q_i)), \quad (5)$$

where h_{ij} is a vector-valued function to be zeroed, H_{0i} is a matrix that maps the generalized coordinates to the actuated angles, h_{ij}^d is a vector-valued function of the desired joint angles (specifically the prosthetic knee q_2 and ankle q_3), and θ_i is the phase variable. The subscript j indicates which leg is in stance, with P indicating that the prosthesis is in stance and C indicating that the contralateral/human leg is in stance (and that the prosthesis is in swing). For the human, a separate output function is defined for the prosthesis single-support period and for the contralateral single-support period, and h_{Hj}^d is encoded using polynomials as in [23]. For the prosthesis, a single, unified output function h_P is defined for the entire stride, i.e., both the stance and swing periods of the prosthesis.

Various torque control methods can be utilized to regulate virtual constraint outputs. Bipedal robots typically enforce virtual constraints using partial (i.e., input-output) feedback linearization [12], which has appealing theoretical properties including exponential convergence [31], reduced-order stability analysis [12], and robustness to model errors [13]. For most of this simulation study, both the prosthesis and the human are controlled using feedback linearization [22], [23]. Note, however, that the prosthesis controller does not depend on the form of the human controller.

The first step in deriving the feedback linearizing controller is differentiating Eq. 5 twice and substituting in the equations of motion (Eq. 1) for \ddot{q}_i to obtain the output dynamics [23]

$$\ddot{y}_{ij} = L_{f_i}^2 h_{ij} + L_{g_i} L_{f_i} h_{ij} \cdot u_i + L_{p_i} L_{f_i} h_{ij} \cdot F + L_{r_i} L_{f_i} h_{ij} \cdot G_i, \quad (6)$$

where Lie derivative notation [31] has been used¹. These terms are given by

$$\begin{aligned} L_{f_i}^2 h_{ij} &= \frac{\partial}{\partial q_i} \left(\frac{\partial h_{ij}}{\partial q_i} \dot{q}_i \right) \dot{q}_i - \frac{\partial h_{ij}}{\partial q_i} M_i^{-1} (C_i \dot{q}_i + N_i), \\ L_{g_i} L_{f_i} h_{ij} &= \frac{\partial h_{ij}}{\partial q_i} M_i^{-1} B_i, & L_{p_i} L_{f_i} h_{ij} &= \frac{\partial h_{ij}}{\partial q_i} M_i^{-1} J_i^T \\ L_{r_i} L_{f_i} h_{ij} &= \frac{\partial h_{ij}}{\partial q_i} M_i^{-1} E_i^T. \end{aligned}$$

The nonlinearities in the output dynamics are canceled by setting the desired output dynamics to $\ddot{y}_{ij} = v_{ij}$, for some PD controller v_{ij} , and solving for the required input torques:

$$u_{ij} = \alpha_{ij} + \beta_{ij} \cdot F + \gamma_{ij} \cdot G_i, \quad (7)$$

where F and G_i are known through measurement, and

$$\begin{aligned} \alpha_{ij} &= [L_{g_i} L_{f_i} h_{ij}]^{-1} (v_{ij} - L_{f_i}^2 h_{ij}), \\ \beta_{ij} &= -[L_{g_i} L_{f_i} h_{ij}]^{-1} \cdot L_{p_i} L_{f_i} h_{ij}, \\ \gamma_{ij} &= -[L_{g_i} L_{f_i} h_{ij}]^{-1} \cdot L_{r_i} L_{f_i} h_{ij}. \end{aligned}$$

The output function h_{ij} is the only term in this control law that can change based on which leg is in stance (indicated by j). The human controller u_{Hj} will utilize different output functions between stance and swing according to [23], [24]. However, the prosthesis will utilize a single output function h_P that does not change between stance and swing. Thus, we can define a unified control law for the prosthesis:

$$u_P = \alpha_P + \beta_P \cdot F + \gamma_P \cdot G_P. \quad (8)$$

It can be difficult to accurately measure the interaction forces F and the ground reaction forces G_P as well as accurately model the $\alpha_P/\beta_P/\gamma_P$ terms for the prosthesis, which may make implementing feedback linearization challenging. An alternative control approach is a linear output PD controller that does not require these modeling terms or force measurements, possibly at the cost of tracking accuracy [22]. In particular, we can approximate the desired feedback linearization by directly generating control torques with the linear input v_P used in Eq. 8. This input is usually defined as an output PD control law, which when used on its own can be interpreted as joint impedance control:

$$u_{imp} = -K_p(H_{0P}q_P - h_P^d(s_P)) - K_d(H_{0P}\dot{q}_P - \dot{h}_P^d(s_P)), \quad (9)$$

where K_p and K_d are gains to control stiffness and damping, respectively. We will demonstrate in Section IV that this control law (Eq. 9) can reasonably enforce the unified virtual constraints with a proper choice of PD gains.

III. UNIFIED VIRTUAL CONSTRAINTS

This section formulates unified virtual constraints using the method of DFT. We then convert piecewise HZD virtual constraints for the model prosthesis of Section II into the unified form and discuss some of the benefits of this parameterization.

¹A Lie derivative $L_f h := \nabla_x h \cdot f$ represents the change of a function $h(x)$ along a vector field $f(x)$. A second-order Lie derivative $L_f^2 h = \nabla_x (L_f h) \cdot f$.

A. Parameterizing Unified Virtual Constraints by DFT

Typically virtual constraints are time-invariant and depend on a phase variable that is unactuated and monotonic [12]. We require the phase variable to be monotonic over the complete stride in order to parameterize a complete joint pattern. For this work, the phase variable was chosen to be the horizontal hip position q_x measured relative to a coordinate frame created at the transition from contralateral stance to prosthesis stance. Other options for the phase variable could also be considered in this framework [21], [32]. For convenience the phase variable $\theta_P(q_P) = q_x$ was normalized between 0 and 1 using

$$s_P(\theta_P(q_P)) = \frac{\theta_P - \theta_P^+}{\theta_P^- - \theta_P^+}, \quad (10)$$

where the ‘+’ signifies the start of the stance period for the prosthetic leg and the ‘-’ indicates the end of its swing period.

Taking advantage of the periodic kinematics observed in human gait [33], the method of DFT can be used to define a unified virtual constraint for each joint. Let $x[n]$ be a discrete signal representing N equally spaced samples of a desired joint trajectory over the phase variable. The DFT is a linear transformation of $x[n]$ into its discrete frequency components

$$X[k] = \sum_{n=0}^{N-1} x[n] W_N^{kn}, \quad k = 0, 1, \dots, N-1, \quad (11)$$

where $W_N = e^{-j(2\pi/N)}$ [25]. Because the signal $x[n]$ is periodic, there are a finite number of discrete frequencies. This signal can then be reconstructed using Fourier Interpolation:

$$x[n] = \frac{1}{N} \sum_{k=0}^{N-1} X[k] W_N^{-kn}, \quad n = 0, 1, \dots, N-1, \quad (12)$$

where $X[k] = \text{Re}\{X[k]\} + j \text{Im}\{X[k]\}$ and $W_N^{-kn} = \text{Re}\{W_N^{-kn}\} + j \text{Im}\{W_N^{-kn}\}$ in standard complex form. Because the joint kinematic signals are real numbers, only the real part of $x[n]$ remains after substitution of $X[k]$ and W_N^{-kn} in Eq. 12 (see [25]). Moreover, the signal reconstruction only requires frequency terms from $k = 0$ to $N/2$ (the Nyquist sampling frequency), beyond which the magnitudes of $X[k]$ and $X[N-k]$ are equal [25]. This results in the following exact representation of the original sampled joint trajectory:

$$x[n] = \frac{1}{2} \alpha_0 + \sum_{k=1}^{\frac{N}{2}-1} \left[\alpha_k \text{Re}\{W_N^{-kn}\} - \beta_k \text{Im}\{W_N^{-kn}\} \right] + \frac{1}{2} \alpha_{\frac{N}{2}} \text{Re}\{W_N^{-\frac{N}{2}n}\}, \quad n = 0, 1, \dots, N-1, \quad (13)$$

where $\alpha_k = 2 \text{Re}\{X[k]\} \in \mathbb{R}$ and $\beta_k = 2 \text{Im}\{X[k]\} \in \mathbb{R}$ are the scalar coefficients based on the original signal.

The Fourier Interpolation in Eq. 13 is used to parameterize the trajectory function h_P^d in Eq. 5 for the entire stride. After computing the coefficients α_k and β_k from a desired joint trajectory (to be specified later), Eq. 13 is expressed as a summation of sinusoids using Euler’s relationship ($e^{\pm j\Omega} = \cos \Omega \pm j \sin \Omega$) in W_N to obtain

$$h_P^d(s_P) = \frac{1}{2} \alpha_0 + \frac{1}{2} \alpha_{\frac{N}{2}} \cos(\pi N s_P) + \sum_{k=1}^K \left[\alpha_k \cos(\Omega_k s_P) - \beta_k \sin(\Omega_k s_P) \right], \quad (14)$$

where $\Omega_k = 2\pi k$ and K is the total number of frequencies (up to $N/2$) used to parameterize the virtual constraint. Eq. 14 is inserted into Eq. 5 to define the virtual constraint output. Because Eq. 14 is composed of sine and cosine functions, the resulting virtual constraints are inherently periodic across the normalized phase variable with a period of one.

B. From HZD to Unified Virtual Constraints

The previous section shows how to encode a given trajectory into a unified virtual constraint but not how to design such a trajectory. In the prosthetic application it is desirable to leverage the provable stability properties of piecewise HZD designs [9], [12]–[19], [23], [24] while respecting the continuous, periodic nature of human walking. Therefore, this section will convert the prosthetic HZD design from [23], [24] into continuous, unified DFT virtual constraints and discuss the fundamental differences between the two approaches.

HZD-based controllers are defined in a piecewise manner, where the virtual constraint depends on which leg is in stance. This allows the controller to respect the discontinuous impact dynamics (Eq. 4), so that if the error just before a properly timed impact is zero, the error just after impact will also be zero. This behavior is called hybrid invariance. Because the DFT parameterization is infinitely smooth and unified across impact events, it cannot be hybrid invariant. By definition these smooth trajectories cannot encode the velocity discontinuities across the impact model. However, the simulations in Section IV will show that the unified DFT controller approximates the stability properties of the piecewise HZD design. Moreover, we will demonstrate the benefits of the unified approach when the impact occurs earlier or later than expected (as is common with human variability [34]), which violates the hybrid invariance assumption of the original HZD design.

The piecewise HZD virtual constraints in [23], [24] are parameterized by the common Bézier polynomial form

$$h_{P,j}^d(s_P) = \sum_{i=0}^Q \frac{a_i Q!}{i!(Q-i)!} s_P^i (1-s_P)^{Q-i}, \quad (15)$$

where j indicates which leg is in stance, $Q = 5$ is the degree of the polynomial, a_i are the polynomial coefficients, and s_P is the normalized phase variable within stance or swing. Hybrid-invariant Bézier polynomials were designed for the knee and ankle to mimic certain features of human walking at various speeds [23], [24], and here we consider the 1.2 m/s design.

In order to create unified virtual constraints, the stance and swing Bézier polynomials were concatenated and sampled to provide one periodic sequence with $N = 1000$ equally spaced data points. The frequency terms $X[k]$ of this sequence were computed by the MATLAB fft function and then used to create the unified DFT function from Eq. 14. The DFT spectrum of these trajectories indicate that the magnitude is approximately zero between the 10th frequency and the Nyquist sampling frequency ($N/2$). As a result, the DFT series can be truncated to reduce the number of coefficients in h_P^d and in turn reduce the computational complexity of the control law (Eq. 8 or 9).

To verify that the first 10 indices accurately represent the desired trajectories, virtual constraints were generated with

TABLE I
FITTING STATISTICS OF DFT DESIGN

K value	Knee		Ankle	
	r^2	RMSE (rad)	r^2	RMSE (rad)
5	0.999	2.23e-04	0.995	1.33e-04
10	1.000	6.14e-05	1.000	3.14e-05
$N/2$	1.000	4.50e-05	1.000	1.17e-05

$K = 5, 10,$ and $N/2$, where K is the highest index k in Eq. 14. As expected the virtual constraints for $K = 10$ and $N/2$ are similar and more accurate than that of $K = 5$ (Table I). The virtual constraints with $K = 5$ have coefficients of determination $r^2 > 0.995$, whereas the $K = 10$ case has $r^2 = 1.000$. In all cases, the root mean square error (RMSE) is less than $2.3\text{e-}04$ rad. From this analysis we can conclude that a 5^{th} - or 10^{th} -order DFT function is sufficient to parameterize the 5^{th} -order Bézier polynomials, so the two approaches will have similar real-time computational costs.

The unified DFT parameterization of the piecewise HZD polynomials provides unique properties that are advantageous for the prosthetic application. The periodic DFT design parameterizes the knee and ankle trajectories across gait cycles, whereas the Bézier polynomials immediately diverge to unbounded values outside the design range of s_P (Fig. 2). Therefore, the piecewise design requires very accurate detection of stance vs. swing, which can be difficult to measure from the limited sensors on a prosthetic leg. Moreover, the strict design range of the Bézier polynomials makes them more sensitive to drift in the phase variable, which must be reset back to zero after every impact event to avoid exceeding the design limits. Practical HZD implementations typically saturate the phase variable at the design limits to prevent undesirable angle commands [14]. In contrast, the DFT design is periodic over the phase variable, so this formulation transitions seamlessly to the next gait cycle. Thus, the phase variable does not necessarily have to be reset or saturated as the amputee transitions from one step to the next, which may simplify the control implementation and lead to more predictable behavior.

In conclusion, piecewise HZD polynomials can be converted to unified DFT virtual constraints with limited coefficients in the output function h_p^d . This method unifies not only a single stride but also periodic steady-state locomotion. In the DFT formulation, the phase variable may only need to be reset across short or long strides to ensure the following stride begins at the proper phase location (modulo the design range of the phase variable). Occasional resets in the phase variable may also be desirable in practice to prevent measurement drift.

IV. SIMULATION RESULTS

This section will demonstrate the ability of the unified prosthetic controller to generate walking gaits that closely match the reference HZD gaits at various design speeds. The benefits of the unified design become clear when hybrid invariance of the piecewise HZD design is violated due to a mismatch with the human controller, specifically in the design speed. We also show numerically that the unified gaits are

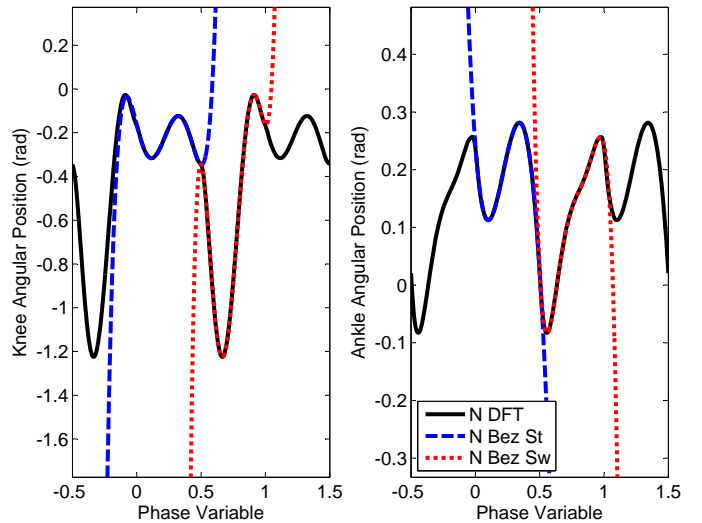


Fig. 2. Virtual constraints by DFT and Bézier polynomial (Bez) for the knee (left) and ankle (right) during normal human walking (N). Because Bézier virtual constraints are defined in a piecewise manner, their normalized phase variable goes from 0 to 1 twice per stride. For comparison, the Bézier phase variable has been scaled and shifted to match the DFT phase variable. The DFT function repeats the gait cycle for phase variable values $s_P < 0$ and $s_P > 1$, i.e., the ranges of $-0.5 \leq s_P < 0$ and $0.5 \leq s_P < 1$ are identical. In contrast, the piecewise Bézier polynomials for stance (St) and swing (Sw) diverge to undesirable trajectories on both sides of the design region.

orbitally stable using either the feedback linearizing controller (Eq. 8) or the impedance controller (Eq. 9).

A. Comparison of Piecewise HZD and Unified DFT

We began with the human and prosthesis HZD designs in [23], [24] for three speeds: normal walking at 1.2 m/s, slow walking at 0.8 m/s and fast walking at 1.6 m/s. Unified DFT virtual constraints were generated for the prosthesis at each speed based on the piecewise Bézier polynomials as described in Section III. For comparison the prosthesis was simulated with either the piecewise HZD virtual constraints or the unified DFT virtual constraints. In all simulations the human part used the piecewise HZD controller for each walking speed and did not change based on the form of the prosthesis controller. The piecewise HZD controllers reset the phase variable at every impact, whereas unified DFT controllers only reset the phase variable at the start of each prosthesis stance period. Both subsystems used the feedback linearizing torque control law (Eq. 7), for which the PD gains were manually tuned and held fixed for all simulations and prosthesis controllers.

Simulations were first performed for the idealized case when both the prosthesis and human had the same desired walking speed. The unified prosthetic controller for each speed tracked the reference HZD virtual constraints very accurately, even across impacts (Fig. 3). Small differences can be observed in the joint velocities (Fig. 4), particularly for the fast walking speed due to larger impact discontinuities. Despite the fact that the unified DFT controller was not hybrid invariant, it performed similarly to the piecewise HZD controller in the ideal case of exactly matched human and prosthesis intent.

Because the intent of the prosthesis and the amputee will rarely be perfectly coordinated, it is critical that the prosthesis

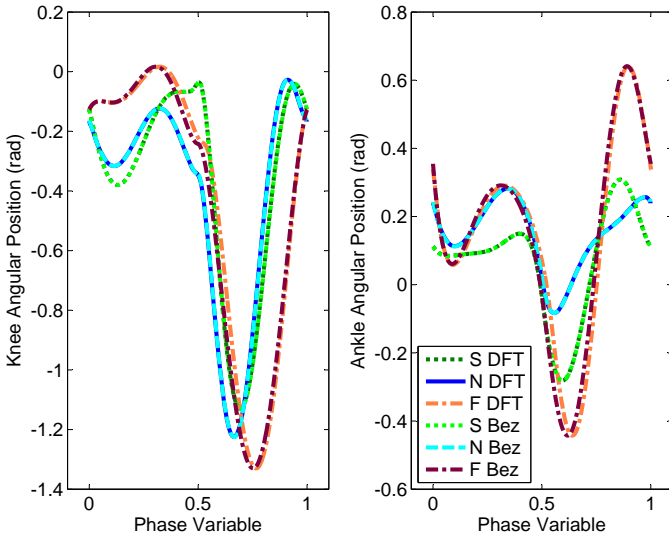


Fig. 3. The simulated trajectories of the prosthetic knee (left) and ankle (right) with both the DFT and Bézier controllers for three different walking speeds (matched with the human speed) plotted against the DFT normalized phase variable. The DFT and Bézier response is almost identical in all cases.

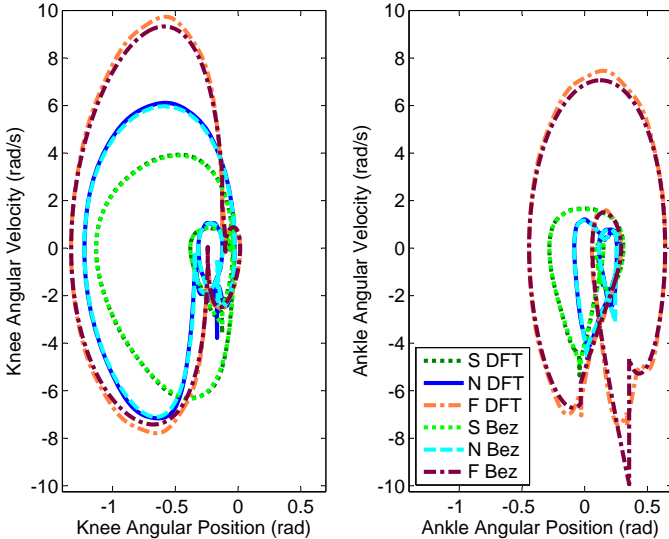


Fig. 4. The simulated phase portrait for the prosthetic knee (left) and ankle (right) for three different walking speeds (matched with human) with the DFT and Bézier controllers. The DFT gaits closely match the reference Bézier gaits. As expected, the greatest deviations occur near impacts. The rolling motion of the curved foot results in a slightly larger ankle orbit for slow walking than normal walking with both controllers.

reacts in a stable and predictable manner to mismatches in the desired walking speed. This is likely to be one of the greatest sources of variability from the human. To test robustness to speed perturbations, the prosthesis controller maintained the normal walking speed while the human controller was set to either slow or fast. Despite these disturbances, the biped converged to steady-state walking for both prosthesis control formulations without any additional tuning. The interaction between the mismatched human and prosthesis resulted in somewhat unexpected changes in speed, although the fast human controller led to faster than normal walking (and

reduced step durations) and the slow human controller led to slower than normal walking (and much longer step durations).

As expected, the mixed speed cases had more tracking error than the matched speed cases (Fig. 5). However, both prosthesis controllers zeroed the tracking error before every impact without requiring unrealistic joint angles or velocities. The two control formulations produced similar torque curves (Fig. 6), which will be discussed later.

In the mixed cases, the Bézier virtual constraints were no longer hybrid invariant, so one of the greatest advantages of the piecewise HZD controller was lost. The transition between strides tended to occur sooner than expected, resulting in discontinuities in the commanded joint angles and thus the tracking errors (and corrective torques). Both controllers had similar errors at the start of prosthesis stance (phase variable from 0 to 0.5), but the unified DFT controller had much smaller errors than the piecewise HZD controller at the start of prosthesis swing (phase variable from 0.5 to 1.0). The small DFT errors may be because the stance-to-swing transition was relatively smooth in velocity, resulting in better tracking from the smooth DFT controller. Further, the DFT phase variable was not reset at the stance-to-swing transition, so a shorter or longer step had less influence on the error. Because the Bézier virtual constraints were defined in a piecewise manner, they were not continuous if the stance-to-swing transition occurred sooner than expected. As a result, the unified controller tracked the desired virtual constraint better than the piecewise HZD controller when the human and prosthesis intent was not exactly matched, as is likely to occur in reality.

B. Stability of Walking Gaits

The local orbital stability for both the matched and mixed speed controllers were analyzed using the method of Poincaré sections [12]. To do so, define the extended state vector from all of the prosthesis and human generalized coordinates as $x_e = (q_e^T, \dot{q}_e^T)^T$, where $q_e = [q_1, q_2, q_3, q_4, q_5, q_6, q_x, q_y]^T$. Walking gaits are cyclic and correspond to solution curves $x_e(t)$ of the hybrid system such that $x_e(t) = x_e(t + T)$, for all $t \geq 0$ and some minimal $T > 0$. These solutions, known as *hybrid periodic orbits*, correspond to equilibria of the Poincaré map $P : G_P \rightarrow G_P$, where the Poincaré section G_P is the set of states corresponding to prosthesis heel strike. The function $P(x_e)$ models two full steps of the biped, mapping the state from a prosthesis impact event to the subsequent prosthesis impact event. A periodic solution $x_e(t)$ then has a fixed point $x_e^* = P(x_e^*)$, about which the Poincaré map can be linearized to analyze local stability. If the eigenvalues are within the unit circle, then the discrete system is locally stable, and we conclude that the hybrid periodic orbit is also locally stable.

In ideal conditions, the hybrid-invariant Bézier polynomials enable an analytical proof of orbital stability with the lower-dimensional HZD [23], [24]. However, hybrid invariance is violated by any mismatch with the human controller, including the mixed speed cases. Moreover, by definition the unified virtual constraints do not satisfy hybrid invariance. Because the analytical HZD result cannot be utilized in these cases, we instead use the perturbation analysis procedure described

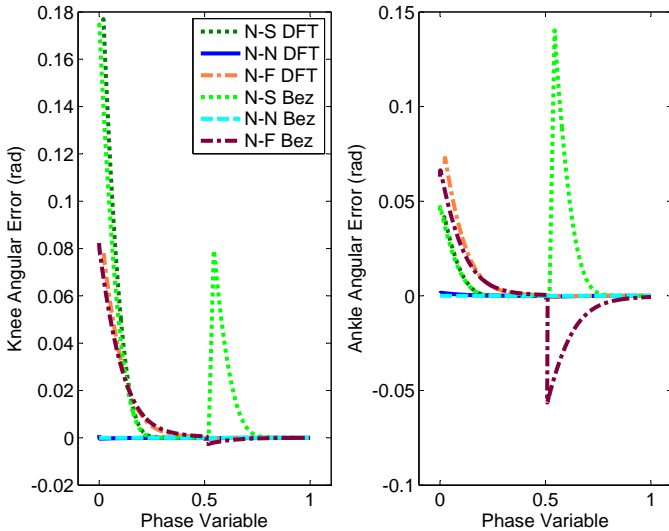


Fig. 5. The simulated tracking errors of the prosthetic knee (left) and ankle (right) for both the unified DFT and piecewise Bézier controllers during steady-state walking with mixed speeds. The normal matched speed error is also shown for comparison. Both controllers have similar error at the start of the stance period (phase variable near 0), but the DFT controller has significantly less error at the start of the swing period (phase variable near 0.5). Note: N-S = normal walking (prosthesis) and slow walking (human), N-N = normal walking (prosthesis) and normal walking (human), and N-F = normal walking (prosthesis) and fast walking (human).

in [35], [36] to numerically calculate these eigenvalues based on simulations. In all cases, the eigenvalues of the linearized map fall within the unit circle (Table II). Thus, the gaits are orbitally stable in the matched and mixed speed cases.

TABLE II
MAXIMUM EIGENVALUES WITH UNIFIED PROSTHETIC CONTROLLER

Prosthetic Leg	Human Model			
	Walking Speeds	Slow	Normal	Fast
	Slow	0.774		
Normal	0.717	0.760	0.639	
Fast				0.758

C. Simulated Walking with Impedance Controller

To apply the feedback linearizing control law (Eq. 8), the dynamics of the prosthesis must be known. Obtaining an accurate dynamic model of the physical system is a challenge in itself. With an uncertain dynamic model and limited sensory feedback for the prosthesis, feedback linearization may be difficult to implement experimentally. A more practical, model-independent implementation is through joint impedance control (Eq. 9), which approximates the torque control inputs for the feedback linearizing controller [22].

This control law was implemented for the prosthesis of the amputee biped model. Noting that real actuators are torque-limited based on the motor and transmission, a saturation limit of ± 120 Nm was implemented for each actuated joint, which is representative of existing powered prosthetic legs [2], [3], [37]. Feedback linearization was still used for the human part of the model, which has been validated as a predictor of certain features of human walking [28], [34]. Using the method

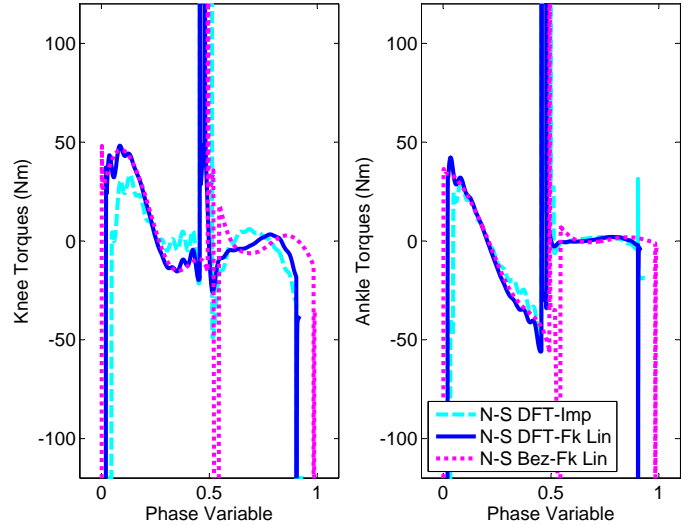


Fig. 6. The simulated torques of the prosthetic knee (left) and ankle (right) for the mixed case of the human at slow speed and the prosthesis at normal speed with the Bézier feedback linearizing controller (N-S Bez-Fk Lin), the DFT feedback linearizing controller (N-S DFT-Fk Lin), and the DFT impedance controller (N-S DFT-Imp). The torques of the impedance controller approximate the feedback linearizing controllers throughout the gait cycle. The torque impulses after impacts are caused by discontinuities in velocity from the impulsive impact model, which do not occur during human walking.

from Section IV-B, the impedance controller was shown to be locally exponential stable with similar eigenvalues to the feedback linearizing controller.

Fig. 6 compares the torques of the impedance controller against the feedback linearizing controllers for both DFT and Bézier in the mixed speed case of normal prosthesis and slow human. The controllers produce similar torques with large spikes just after the discontinuous impact events, which can only be achieved with ideal actuators in simulation. This could potentially be addressed through the use of correction polynomials as in [38]. However, step transitions in human walking are continuous over a double-support period, so these discontinuities will not occur in practice (see [22], [37]). These results demonstrate the feasibility of a model-independent controller for practical implementation in a powered prosthesis.

V. CONCLUSIONS

We developed a single, unified prosthesis controller that captures the entire gait cycle through DFT virtual constraints. The unified controller eliminates the need to divide the gait into different periods with independent controllers. Since the DFT virtual constraint is periodic, the controller does not need to be reset at the start of each stride.

The feasibility of the controller was demonstrated using simulations of an amputee walking model. Three distinct walking speeds were designed and simulated. In all cases, stable periodic gaits emerged. Robustness to speed uncertainty was demonstrated by using a fixed prosthesis controller while the human controller was varied. These mixed speed cases produced stable walking, demonstrating that a single, unified controller can accommodate a range of human walking speeds.

A model-independent impedance controller was also evaluated, demonstrating the viability of implementing the unified control method in hardware.

This control strategy was recently implemented on a powered knee-ankle prosthesis in [37]. Experiments validated the ability of the unified control approach to handle various walking speeds (0-3 miles/hr) in a continuous sequence. Unified virtual constraints could be defined for various activities with well-characterized joint kinematics (e.g., from able-bodied data [33], [39] or model-based optimization [9], [19]). Future experiments will attempt to demonstrate clinical viability by allowing clinicians to visually modify trajectories while configuring the control system for different amputee subjects.

REFERENCES

- [1] M. A. Holgate, T. G. Sugar, and A. Bohler, "A novel control algorithm for wearable robotics using phase plane invariants," in *IEEE Int. Conf. Robot. Automat.*, 2009, pp. 3845–3850.
- [2] F. Sup, A. Bohara, and M. Goldfarb, "Design and control of a powered transfemoral prosthesis," *Int. J. Robot. Res.*, vol. 27, no. 2, pp. 263–273, 2008.
- [3] S. K. Au and H. Herr, "Powered ankle-foot prosthesis," *IEEE Robot. Automat. Mag.*, vol. 15, no. 3, pp. 52–59, 2008.
- [4] M. R. Tucker, J. Olivier, A. Pagel, H. Bleuler, M. Bouri, O. Lamberg, J. del R Millán, R. Riener, H. Vallery, and R. Gassert, "Control strategies for active lower extremity prosthetics and orthotics: a review," *Journal of Neuroengineering and Rehabilitation*, vol. 12, no. 1, 2015.
- [5] M. F. Eilenberg, H. Geyer, and H. Herr, "Control of a powered ankle-foot prosthesis based on a neuromuscular model," *IEEE Trans. Neural Syst. Rehab. Eng.*, vol. 18, no. 2, pp. 164–173, 2010.
- [6] F. Sup, H. A. Varol, and M. Goldfarb, "Upslope walking with a powered knee and ankle prosthesis: initial results with an amputee subject," *IEEE Trans. Neural Syst. Rehab. Eng.*, vol. 19, no. 1, pp. 71–78, 2011.
- [7] B. Lawson, H. Varol, A. Huff, E. Erdemir, and M. Goldfarb, "Control of stair ascent and descent with a powered transfemoral prosthesis," *IEEE Trans. Neural Syst. Rehab. Eng.*, vol. 21, no. 3, pp. 466–473, 2013.
- [8] A. Shultz, B. Lawson, and M. Goldfarb, "Running with a powered knee and ankle prosthesis," *IEEE Trans. Neural Syst. Rehab. Eng.*, vol. 23, no. 3, pp. 403–412, 2015.
- [9] H. Zhao, J. Horn, J. Reher, V. Paredes, and A. D. Ames, "First steps toward translating robotic walking to prostheses: a nonlinear optimization based control approach," *Autonomous Robots*, 2016.
- [10] N. P. Fey, A. Simon, A. J. Young, and L. J. Hargrove, "Controlling knee swing initiation and ankle plantarflexion with an active prosthesis on level and inclined surfaces at variable walking speeds," *IEEE J. Trans. Eng. Health Med.*, vol. 2, pp. 1–12, 2014.
- [11] A. M. Simon, K. A. Ingraham, N. P. Fey, S. B. Finucane, R. D. Lipschutz, A. J. Young, and L. J. Hargrove, "Configuring a powered knee and ankle prosthesis for transfemoral amputees within five specific ambulation modes," *PLoS ONE*, vol. 9, no. 6, p. e99387, 2014.
- [12] E. Westervelt, J. Grizzle, C. Chevallereau, J. Choi, and B. Morris, *Feedback Control of Dynamic Bipedal Robot Locomotion*. Boca Raton, Florida: CRC Press, 2007.
- [13] K. Sreenath, H.-W. Park, I. Poulakakis, and J. Grizzle, "A compliant hybrid zero dynamics controller for stable, efficient and fast bipedal walking on MABEL," *Int. J. Robot. Res.*, vol. 30, no. 9, pp. 1170–1193, 2011.
- [14] A. E. Martin, D. C. Post, and J. P. Schmiedeler, "Design and experimental implementation of a hybrid zero dynamics-based controller for planar bipeds with curved feet," *Int. J. Robot. Res.*, vol. 33, no. 7, pp. 988–1005, 2014.
- [15] A. Ramezani, J. Hurst, K. Hamed, and J. Grizzle, "Performance analysis and feedback control of ATRIAS, a three-dimensional bipedal robot," *ASME J. Dyn. Sys. Meas. Control*, vol. 136, no. 2, p. 021012, 2013.
- [16] B. Buss, A. Ramezani, K. Hamed, B. Griffin, K. Galloway, and J. Grizzle, "Preliminary walking experiments with underactuated 3d bipedal robot MARLO," *IEEE Int. Conf. Intell. Robots Syst.*, 2014.
- [17] K. A. Hamed, B. G. Buss, and J. W. Grizzle, "Continuous-time controllers for stabilizing periodic orbits of hybrid systems: Application to an underactuated 3D bipedal robot," in *IEEE Conf. Decis. Control*, 2014, pp. 1507–1513.
- [18] Q. Nguyen and K. Sreenath, "L1 adaptive control for bipedal robots with control Lyapunov function based quadratic programs," in *Amer. Contr. Conf. IEEE*, 2015, pp. 862–867.
- [19] K. Hamed and R. D. Gregg, "Decentralized feedback controllers for robust stabilization of periodic orbits of hybrid systems: Application to bipedal walking," *IEEE Trans. Control Syst. Tech.*, 2016.
- [20] R. D. Gregg, E. Rouse, L. Hargrove, and J. Sensinger, "Evidence for a time-invariant phase variable in human ankle control," *PLoS ONE*, vol. 9, no. 2, p. e89163, 2014.
- [21] D. J. Villarreal, H. Poonawala, and R. D. Gregg, "A robust parameterization of human joint patterns across phase-shifting perturbations," *IEEE Trans. Neural Syst. Rehab. Eng.*, 2016.
- [22] R. D. Gregg, T. Lenzi, L. Hargrove, and J. Sensinger, "Virtual constraint control of a powered prosthetic leg: From simulation to experiments with transfemoral amputees," *IEEE Trans. Robot.*, vol. 30, no. 6, pp. 1455–1471, 2014.
- [23] A. E. Martin and R. D. Gregg, "Hybrid Invariance and Stability of a Feedback Linearizing Controller for Powered Prostheses," in *Amer. Contr. Conf.*, Chicago, IL, 2015, pp. 4670–4676.
- [24] —, "Stable, robust hybrid zero dynamics control of powered lower-limb prostheses," *IEEE Trans. Autom. Control*, 2017, in press.
- [25] A. V. Oppenheim, R. W. Schafer, and J. R. Buck, *Discrete-Time Signal Processing*. Upper Saddle River, New Jersey: Prentice-Hall Englewood Cliffs, 1989, vol. 2.
- [26] J. Kerestess, T. G. Sugar, and M. Holgate, "Adding and subtracting energy to body motion: Phase oscillator," in *ASME Int. Design Eng. Tech. Conf. & Comp. and Info. in Eng. Conf.*, 2014, p. V05AT08A004.
- [27] D. Quintero, A. E. Martin, and R. D. Gregg, "Unifying the gait cycle in the control of a powered prosthetic leg," in *IEEE Int. Conf. Rehab. Robot.*, 2015, pp. 289–294.
- [28] A. Martin and J. Schmiedeler, "Predicting human walking gaits with a simple planar model," *J. Biomech.*, vol. 47, no. 6, pp. 1416–21, 2014.
- [29] A. H. Hansen, D. S. Childress, and E. H. Knox, "Roll-over shapes of human locomotor systems: Effects of walking speed," *Clin. Biomech.*, vol. 19, no. 4, pp. 407–14, 2004.
- [30] —, "Prosthetic foot roll-over shapes with implications for alignment of trans-tibial prostheses," *Prosth. Orth. Int.*, vol. 24, no. 3, pp. 205–15, 2000.
- [31] A. Isidori, *Nonlinear Control Systems*, 3rd ed. London, England: Springer, 1995.
- [32] D. J. Villarreal and R. D. Gregg, "Unified phase variables of relative degree two for human locomotion," in *IEEE Eng. Med. Bio. Conf.*, 2016.
- [33] D. Winter, *Biomechanics and Motor Control of Human Movement*. Hoboken, New Jersey: John Wiley and Sons, Inc, 2009.
- [34] A. Martin and R. D. Gregg, "Incorporating human-like walking variability in an HZD-based bipedal model," *IEEE Trans. Robotics*, vol. 32, no. 4, pp. 943–948, 2016.
- [35] A. Goswami, B. Thuilot, and B. Espiau, "A study of the passive gait of a compass-like biped robot: Symmetry and chaos," *Int. J. Robot. Res.*, vol. 17, no. 12, pp. 1282–1301, 1998.
- [36] R. D. Gregg, Y. Y. Dhaher, A. Degani, and K. M. Lynch, "On the mechanics of functional asymmetry in bipedal walking," *IEEE Trans. Biomed. Eng.*, vol. 59, no. 5, pp. 1310–1318, 2012.
- [37] D. Quintero, D. J. Villarreal, and R. D. Gregg, "Preliminary experiments with a unified controller for a powered knee-ankle prosthetic leg across walking speeds," in *IEEE/RSJ Int. Conf. Intell. Robots Syst.*, 2016.
- [38] C. Chevallereau, J. W. Grizzle, and C. Shih, "Asymptotically stable walking of a five-link underactuated 3D bipedal robot," *IEEE Trans. Robot.*, vol. 25, no. 1, pp. 37–50, 2008.
- [39] K. R. Embry, D. J. Villarreal, and R. D. Gregg, "A unified parameterization of human gait across ambulation modes," in *IEEE Eng. Med. Bio. Conf.*, 2016.